Energy Research Journal

Original Research Paper

Geometry Modification of Flywheels and its Effect on Energy Storage

Shenel Bankston and Changki Mo

School of Mechanical and Materials Engineering,
Washington State University Tri-Cities, 2710 Crimson Way, Richland, USA

Article history
Received: 01-11-2014
Revised: 12-6-2015
Accepted: 25-08-2015

Corresponding Author:
Changki Mo
School of Mechanical and Materials Engineering,
Washington State University Tri-Cities, 2710 Crimson Way, Richland, USA
E-mail: changki.mo@tricity.wsu.edu

Abstract: This paper examines the influence of various geometric configurations of flywheels on kinetic energy storage performance using finite element analysis. Historically flywheels have been used in various applications. From such applications as pottery wheels to steam engines, flywheels have been used to store mechanical energy. Currently, in the ever expanding world of green energy development, flywheel energy storage systems provide an alternative source of energy storage that does not harm the surrounding environment. But when it comes to overall efficiency, e.g., manufacturing, reduced energy loss, in providing energy to the public, there is always a need for a more cost effective energy storage system. As such, this paper analyzes various geometric configurations of flywheels for the purposes of utilization as an energy storage source alternative. In particular, this is focused on the fact that reducing the amount of materials needed to produce the greatest amount of energy, i.e., high energy density, is needed for a flywheel energy storage system. In the analysis, the key parameters for each flywheel configuration are considered to examine the flywheel energy storage performance. These parameters are polar moment of inertia for determining the energy capacity of the flywheel, the shape factor for each cross section and maximum stress in the flywheel with its corresponding maximum angular velocity for each cross section. With all analytical results in terms of those parameters, an optimal flywheel system will be determined.

Keywords: Flywheel Energy Storage, Polar Moment of Inertia, Finite Element Analysis, Shape Factor

Introduction

The need for alternative energy is very important. For decades, nations have been dependent on fossil fuels as their major energy source. With nonrenewable energy sources such as oil, coal and natural gas depleting, alternative, renewable energy sources such as wind and solar have become a popular research area of interest. Because fossil fuels are currently the cheapest sources of energy in terms of cost and accessibility, wind and solar are slow in becoming a commercially and globally accepted source of energy. Despite the slow acceptance of alternative energy sources, the rising costs of fossil fuels will ultimately make alternative energy sources the norm.

Although wind and solar are major potential sources of energy, they are, by their nature intermittent in power production. Wind and solar power are not produced steadily since they are dependent on seasonal changes (Kousksou *et al*., 2014). New forms of energy storage are needed to support these alternative energy systems. The ability to store energy from these alternative energy sources would allow excess energy to be stored and released during peak use times, or when weather would not allow energy use from the primary source (Kousksou *et al*., 2014). The most well-known energy storage device used today is the electric battery. An electric battery is a device consisting of one or more electrochemical cells that convert stored chemical energy into electrical energy. Although batteries have been used for years in everything from cars to laptop computers, they are not the ideal energy storage system for storing energy from wind and solar mainly due to their short life cycle and chemical degradation over time. Storing energy via a flywheel using kinetic energy is a more efficient and less wasteful alternative to energy storage by electrochemical means.

Science Publications

© 2015 Shenel Bankston and Changki Mo. This open access article is distributed under a Creative Commons Attribution (CC-BY) 3.0 license.

DOI: 10.3844/erjsp.2015.54.63

A flywheel is a rotating disk that can store or dissipate, mechanical, kinetic energy utilizing rotary inertia. The three major elements that will determine the energy storage capacity and efficiency from the flywheel storage systems are (Arslan, 2008):

- Strength of material used-stronger materials can take larger stresses and therefore can be operated at higher speeds
- Geometric profile of flywheel (shape factor, *K*)-geometry of the disk (polar moment of inertia) is proportional to the energy generation of the flywheel system
- Rotational speed-the square of the rotational speed is proportional to the energy generation of the flywheel system, even more so than the geometry

The goal of this paper is to manipulate the geometry of two different types of flywheels through quasi-parametric methods to obtain a high energy storage capacity and high shape factor value.

Historical and Present Uses of Flywheels

Historically, the use of flywheels was an everyday activity. During prehistoric times, rotary inertia was advantageous in making fire and for boring through objects like rock and wood. Genta (1985) provides a detailed, historical reference of the many innovative uses of rotary energy and flywheels during different periods of history. During the industrial revolution, the use of flywheels was mainly used to maintain vibration stability and balance in machines and engines (Bitterly, 1998). Starting in the 1960s, flywheel storage systems were proposed in some NASA sponsored programs, for use as primary energy storage sources during space missions (Moore and Kraft, 2012). More modern uses of flywheels include: Regenerative braking systems for electric cars (Liu and Jiang, 2007; Moore and Kraft, 2012; Pochiraju, 2012), aerospace applications (Moore and Kraft, 2012) and high energy producing flywheel storage systems.

Over the last 30 years the development of microelectronics, magnetic bearing systems and high power density motor-generators have enabled more research into the use of flywheel energy storage capabilities to be a viable alternative, renewable energy storage device (Bitterly, 1998).

Parts of a Flywheel Storage System

As shown in Fig. 1, there are several main elements to a flywheel storage system. A simple flywheel storage system consists of a flywheel, bearings, flywheel housing, motor- generator and motor control systems (not shown).

The type of bearings and housing chosen for the flywheel storage system is essential to decrease energy loss through air and mechanical friction and for providing a safe environment to operate the system. Mechanical bearings are not ideal due to high energy loss due from friction and the need for lubrication and periodic maintenance. Because of this, more modern flywheel storage systems use magnetic bearings to levitate the shaft to reduce the need for lubrication and to reduce energy loss from friction (Pena-Alzola *et al*., 2011). The housing prevents loss of energy from air friction. Air friction torque is proportional to rotational speed of the system. To reduce the energy loss from air friction, flywheel storage systems are placed in a vacuum housing. The housing must also be able to confine any possible fragments in the case of a flywheel being operated past its designed speed. It is recommended that the flywheel housing be at least half the weight of the flywheel, for high speed flywheels and 2.5 times the weight of the flywheel for low speed applications (Pena-Alzola *et al*., 2011). The motor-generator can either apply energy to the system, in the form of torque, to gain kinetic energy, or used as generator to convert the kinetic energy stored in the flywheel into electric energy (Bolund *et al*., 2007).

The results presented in this study assume the following conditions:

- Frictionless support
- Vacuum housing
- No energy loss to environment

There are two commonly used types of flywheel storage systems in industry: Steel flywheels that run at speeds less than 6000 rpm and composite flywheels, e.g. carbon fiber, that run at speeds between 10,000 and 100,000 rpm. Because flywheel fabricated from composite materials are beyond the scope of this paper, only structural steel will be used in all analysis performed in this study.

Flywheel Storage System Advantages and Disadvantages

Some flywheel storage system advantages are (Bolund *et al*., 2007):

- High power density potential
- No capacity degradation, long life expectancy
- Safe for the environment, non-toxic
- Low maintenance over its lifetime

Some disadvantages are (Genta, 1985):

- Safety due to high speed operations
- Fatigue due to stop/start, high/low flywheel operations

Stress fluctuations

- Vibration cause by flywheel imbalance

DOI: 10.3844/erjsp.2015.54.63

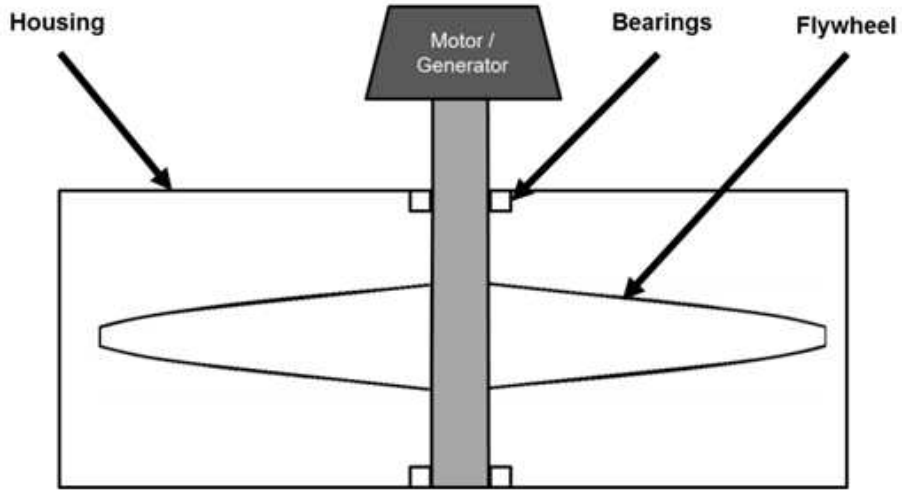

Fig. 1. Simple flywheel storage system configuration

Nomenclature

c_1, c_2:	Constants of integration
E:	Energy
E_Y:	Elastic modulus
e_m:	Energy per unit mass, specific energy
e_v:	Energy per unit volume, specific energy
h:	Constant of disk profile
J:	Polar moment of inertia
K:	Shape factor
m:	Mass
m_1, m_2:	Constants
r:	Radius of disk
r_a:	Inner radius of disk from axis of rotation
r_b:	Outer radius of disk from axis of rotation
s:	Exponential constant of disk profile
t(r):	Thickness at radius, r
t_a:	Thickness at r_a
t_b:	Thickness at r_b
V:	Volume

Greek Symbols

ν:	Poisson's ratio
ρ:	Density of material
σ_{ult}:	Ultimate stress of a material
σ_r:	Radial stress
σ_r^*:	ANSYS generated radial stress
σ_θ:	Hoop stress
σ_θ^*:	ANSYS generated hoop stress
$\sigma_{\omega_{@K=1}}$:	Hoop stress at $\omega_{@K=1}$
ω:	Rotational velocity
$\omega_{@K=1}$:	Rotational velocity at K=1
ω_{max}:	Maximum rotational velocity for a specific shape and material

Methodology for Determining Optimal Flywheel Profile

This paper analyzes flywheel profiles based on the shapes shown in Figs. 2 and 3. Figure 2 was chosen based on a common flywheel shape: the thick rimmed flywheel. The profile in Fig. 2 has most of its mass concentrated on the outer radius. Figure 3 is essentially the reversed or flipped cross sectional profile of Fig. 2.

Equation (1) is the mathematical representation of the thickness profile for both Figs. 2 and 3 (Ugural and Fenster, 2011). In developing a set of stress equations to solve for flywheels with the shapes given in Figs. 2 and 3, Ugural and Fenster (2011) used the shape shown in Fig. 3 as a template to set up the stress equations. Equation (1) can be manipulated and used to describe the profile in Fig. 2 in order to be used with the same stress equations. The value of *s* becomes positive with Profile #1 and negative with Profile #2. Equations (2) and (3), which are dependent on the shape of the profile, are derived from Ugural and Fenster (2011):

$$t(r) = h \cdot r^{-s} \tag{1}$$

Where

$$s = \frac{\ln \frac{t_b}{t_a}}{\ln \frac{r_b}{r_a}} \tag{2}$$

$$h = \frac{t_b}{r_b^{-s}} \tag{3}$$

DOI: 10.3844/erjsp.2015.54.63

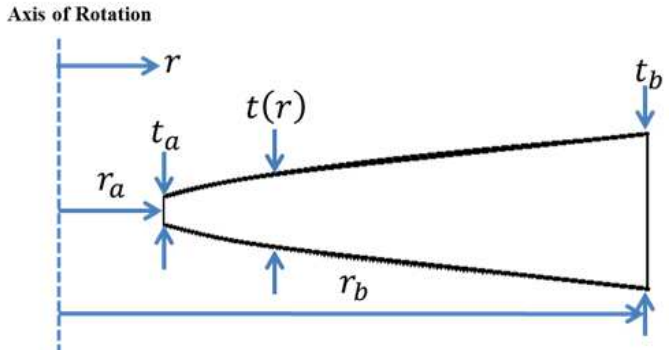

Fig. 2. Flywheel profile #1

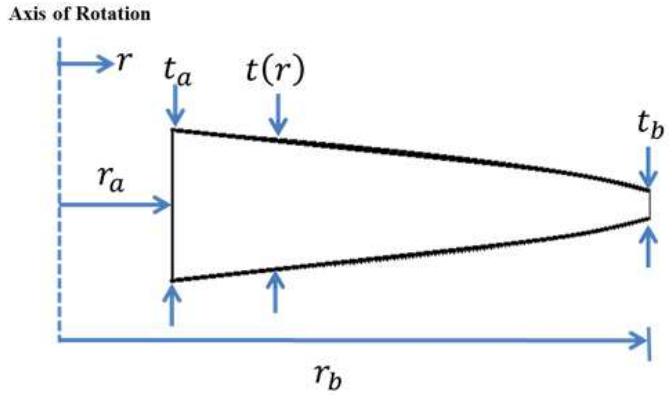

Fig. 3. Flywheel profile #2

Equations (2) and (3) are mathematical definitions of the constants identified in Equation (1). Tables 1 and 2 list the different combinations of t_a, t_b, r_a and r_b used for this analysis. Although all of the numbers look arbitrary, the numbers were picked based on different ratios of t_a/t_b, r_b/t_a and r_b/t_a in the case of Profile # 2. Two t_a/t_b ratios, 0.10 and 0.83 were selected because they fall between 0 and 1. Zero being an infinitely small t_a, to 1 being a flat disk profile. Different values of r_b/t_b were chosen due to the uncertainty of plane stress being applicable to certain profiles. Ratios of 8 to 1, 6 to 1, 4 to 1 and 2 to 1 were chosen to determine which range of ratios would be applicable to the set of stress equations in the next section. $r_a = 0.03$ m and $r_b = 0.51$ m are the inner and outer radius, respectively, for all of the evaluated sections. The values for *h* and *s* were solved based on the combinations of t_a, t_b, r_a and r_b. Setting up an array of profiles in this manner will provide a quasi-parametric analysis that can be used for a variety of different thicknesses and radii.

Hoop and Radial Stress Equations for a Rotating Disk of Variable Thickness

Equation (4) is the governing equation for the stress distribution in a disk of variable thickness (Ugural and Fenster, 2011).

$$\frac{d}{dt}\left[t(r)r\sigma_r\right]-t(r)\sigma_\theta+t(r)\rho\omega^2r^2=0 \tag{4}$$

Equation (4) is valid as long as profile, $t(r)$, meets the assumption of plane stress, i.e. $t_b<<r_b$ (You *et al*., 2000). The solution to Equation (4) is fully derived in Ugural and Fenster (2011). The final solution for radial and hoop stress are expressed in Equations (5) and (6).

Equation (6), hoop stress, is of particular interest because it is the highest stress generated in a spinning disk; therefore it is the stress that will ultimately determine how fast the flywheel can operate before failure:

$$\sigma_r=\frac{c_1}{h}r^{m_1+s-1}+\frac{c_2}{h}r^{m_2+s-1}-\frac{3+\nu}{8-(3+\nu)s}\rho\omega^2r^2 \tag{5}$$

$$\sigma_\theta=\frac{c_1m_1}{h}r^{m_1+s-1}+\frac{c_2m_2}{h}r^{m_2+s-1}-\frac{1+3\nu}{8-(3+\nu)s}\rho\omega^2r^2 \tag{6}$$

Where:

$$m_1,m_2=-\frac{s}{2}\pm\sqrt{\left(\frac{s}{2}\right)^2+(1+\nu s)} \tag{7}$$

Table 1. Parameters for flywheel profile #1

Case #	t_am	t_bm	t_a/t_b	r_b/t_a	s	h
1	0.051875	0.06250	0.83	8	-0.06	2.08
2	0.006250	0.06250	0.10	8	-0.77	0.25
3	0.069098	0.08325	0.83	6	-0.06	2.76
4	0.008250	0.08325	0.10	6	-0.77	0.33
5	0.103750	0.12500	0.83	4	-0.06	4.15
6	0.012500	0.12500	0.10	4	-0.77	0.50
7	0.207500	0.25000	0.83	2	-0.06	8.30
8	0.025000	0.25000	0.10	2	-0.77	1.00

Table 2. Parameters for flywheel profile #2

Case #	t_am	t_bm	t_a/t_b	r_b/t_a	s	h
9	0.06250	0.051875	1.2	8	0.06	2.50
10	0.06250	0.006250	10.0	8	0.77	2.50
11	0.08325	0.069098	1.2	6	0.06	3.33
12	0.08325	0.008325	10.0	6	0.77	3.33
13	0.12500	0.103750	1.2	4	0.06	5.00
14	0.12500	0.012500	10.0	4	0.77	5.00
15	0.25000	0.207500	1.2	2	0.06	10.00
16	0.25000	0.025000	10.0	2	0.77	10.00

Equation (7) is developed based on the method used to solve Equation (4) (Ugural and Fenster, 2011). C_1 and c_2 are determined from the boundary condition:

$$\sigma_{r_{@r=a}} = \sigma_{r_{@r=b}} = 0$$

Although the scope of this paper is focused on the use of ANSYS to determine the stresses in complex flywheel profiles, Equations (5) and (6) were included to not only represent the theory behind the solutions obtained by ANSYS, but also used to verify by comparison, which profiles are applicable to Equations (5) and (6) due to the thickness limitation on those equations.

Energy and Shape Factor Equations

Equation (8) is the energy stored/released in a flywheel:

$$E = \frac{1}{2} J\omega^2 \tag{8}$$

Where:

$$J = \int r^2 dm \tag{9}$$

Or:

$$J = \int_{r_a}^{r_b} 2\pi\rho r^3 t(r) dr \tag{10}$$

Where:

$$dm = \rho dV \text{ and } dV = 2\pi r t(r) dr$$

Equation (10) is derived from both the definition of polar moment of inertia and the cylindrical shell method for calculating volume.

Shape factor, K, is only dependent on the polar moment of inertia. The shape factor, usually, ranges between 0.3 and 1.0. In reality, it is impossible to obtain a factor of 1.0 (Arslan, 2008). The shape factor can be associated with the efficiency of the system due to the fact that when 100% specific energy from the material can be converted to specific energy from the shape and mass, K is equal to 1. In order to find K for each profile case, the equation to determine specific energy, Equation (11) or (12), is used (Bolund *et al*., 2007):

$$e_V = \frac{E}{V} = K\sigma_{ult} \tag{11}$$

Or:

$$e_m = \frac{E}{m} = K\frac{\sigma_{ult}}{\rho} \tag{12}$$

To solve for the maximum operating speed, ω_{max}, for each disk shape and material, Equations (13) through (16) are used.
For $K = 1$:

$$\frac{E}{m} = \frac{\sigma_{ult}}{\rho} \tag{13}$$

Solving for ω:

$$\omega_{@K=1} = \sqrt{\frac{2\sigma_{ult}}{\rho J}} \tag{14}$$

This value is used as an input to Equations (5) and (6) to solve for σ_θ which is the dominating stress in determining the ultimate speed at which the flywheel can operate.

To solve for actual value of *K*:

$$K = \frac{\sigma_{ult}}{\sigma_{\omega_{@K=1}}} \tag{15}$$

To solve for the true maximum operating speed of the flywheel, ω_{max}, Equation (16) is used:

$$\omega_{\max} = \sqrt{K} \cdot \omega_{@K=1} \tag{16}$$

Equations (13) through (16) are used as an expedient method of solving for the exact, maximum operating speed without using reiterative means of cycling through Equations (5) and (6) until an exact solution is obtained.

Results

All of the ANSYS results shown below were analyzed using 5000 rpm and structural steel (ν = 0.3, E_Y = 200 GPa, ρ = 8027.20 kg/m^3) as a basis to compare with the analytical results from Equations (5) and (6). All of the models are three dimensional and uses SOLID 187 elements which are 10 node elements having three translational, degrees of freedom at each node. A default constraint, placed on the inner face of the central hole, was used instead of a fixed or frictionless support. When ANSYS detects a rigid body displacement during the analysis, weak springs placed where it would prevent a rigid body movement due to the applied force. Based on these inputs, Figures 4 through 8 were obtained. It is noted that only some hoop stress results are shown. The remaining values obtained from ANSYS are shown in Tables 3 and 4.

In Tables 3 and 4, results from ANSYS are compared with results from Equations (5) and (6). All results use structural steel rotated at 5000 rpm. Although the results surpass the ultimate strength of structural steel, 460.01 MPa, these values are only meant to calculate the percent difference between ANSYS values and values obtained from Equations (5) and (6). Negative percent differences mean ANSYS values were more conservative and positive values mean Equations (5) and/or (6) are more conservative. Stress values with an asterisk are values obtained from ANSYS.

Based on the percent differences shown in Tables 3 and 4, cases where the percent differences are below 50% difference, Equations (5) and (6) will not be used to calculate the shape factors. Equations (13) through (16), along with ANSYS, will be used to calculate the shape factor for those profiles whose percent differences are over 50%. It is noted that Tables 3 and 4 primarily deal with percent differences.

Discussion

According to the solutions provided in Table 5, Profile #2 in Fig. 3 is the most efficient due to its higher shape factor values. However, despite having larger shape factor values, Profile #1 in Fig. 2, has the larger energy storage capacity in some cases of the two profiles. For example, if one chose case #16, although its shape factor is higher case #16 would not have as much energy storage capacity as case #15, because:

$$26{,}387{,}087.77 \times 0.33 = 8{,}707{,}738.96\ \text{N}\cdot\text{m}$$
$$> 5{,}980{,}916.13 \times 0.40 = 2{,}392{,}366.45\ \text{N}\cdot\text{m}$$

Choosing the much heavier flywheel would have the best energy capacity between these profiles.

Different constraints that are chosen in the ANSYS analysis will produce different results. In some cases the frictionless supports gave some better percent differences between the ANSYS results and the analytical results. In other cases a fixed constraint provided some better percent difference than what Tables 3 and 4 shows. But overall, the weak spring support provided the best values in terms of percent differences across the board. Depending on the actual system and constraints, the shape factors may be different.

Although structural steel, which has a very low strength to weight ratio, was chosen as the material for analysis, it can be shown that a material such as titanium, which has high strength to weight ratio, has an even higher energy storage capacity than that shown in Table 5. This does not change the shape factor of the flywheel. The shape factor is solely dependent on the physical aspects of the flywheel, i.e., polar moment of inertia. There are ongoing studies on mixed carbon fiber/steel flywheel that have the ability to operate with speed up to 10,000 rpm, which at any flywheel shape that is chosen, will store large amounts energy despite the shape of the flywheel.

Equations (13) though (16) are very useful equations for solving for the shape factor for any flywheel shape that is analyzed without the use of a complex analytical equation. Instead of inputting $\omega@_{K=1}$ into Equations (5) and (6), $\omega@_{K=1}$ can be used as an input into ANSYS or whatever stress analysis software that is being used and will produce a corresponding hoop stress that can be used in the remaining equations.

As shown in Tables 3 and 4, a method utilizing thickness ratios, e.g., t_a/t_b = 1.2, provides for a parametric system to chose different sizes of thickness. Table 3, for example, demonstrates that for whatever value is chosen for t_a and t_b, the ratio of the two, whether it be 0.83 or 0.10, will generate the stress value for the same ratio but with different t_a and t_b, therefore reducing the amount of data that needs to be analyzed.

DOI: 10.3844/erjsp.2015.54.63

Table 3. Percent difference between analytical and ANSYS results for profile #1

Case #	t_am	t_bm	t_a/t_b	σ_r, MPa	σ_r*, MPa	% difference	σ_θ, MPa	σ_θ*, MPa	(%) difference
1	0.051875	0.0625	0.83	219.55	218.05	0.68%	510.84	498.1	2.49
2	0.00625	0.0625	0.1	356	425.12	-19.42%	1226.47	1286.77	-4.92
3	0.069098	0.08325	0.83	219.55	219.4	0.07%	510.84	516.01	-1.01
4	0.00825	0.08325	0.1	356	410.44	-15.29%	1226.47	1277.12	-4.13
5	0.10375	0.125	0.83	219.55	221.65	-0.96%	510.84	544.69	-6.63
6	0.0125	0.125	0.1	356	404.09	-13.51%	1226.47	1287.39	-4.97
7	0.2075	0.25	0.83	219.55	226.87	-3.33%	510.84	532.45	-4.23
8	0.025	0.25	0.1	356	429.54	-20.66%	1226.47	1259.05	-2.66

Table 4. Percent difference between analytical and ANSYS results for profile #2

Case #	t_am	t_bm	t_a/t_b	σ_r, MPa	σ_r*, MPa	(%) difference	σ_θ, MPa	σ_θ*, MPa	(%) difference
9	0.06250	0.051875	1.2	203.96	198.77	2.55	429.66	435.60	-1.38
10	0.06250	0.006250	10.0	149.60	121.28	18.93	149.53	257.89	-72.46
11	0.08325	0.069098	1.2	203.96	201.19	1.36	429.66	425.95	0.86
12	0.08325	0.008325	10.0	149.60	120.83	19.23	149.53	252.33	-68.74
13	0.12500	0.103750	1.2	203.96	201.34	1.28	429.66	439.00	-2.17
14	0.12500	0.012500	10.0	149.60	121.02	19.10	149.53	251.13	-67.95
15	0.25000	0.207500	1.2	203.96	204.94	-0.48	429.66	456.10	-6.15
16	0.25000	0.025000	10.0	149.60	121.28	18.93	149.53	278.29	-86.11

Table 5. Energy and shape factor for profiles #1 and #2-structural steel

					Structural steel					
Case #	t_a, m	t_b, m	t_a/t_b	ω_{max}, rpm	$\omega_{K=1}$, rpm	mass, kg	σ_{ult}, MPa	J, kg.m^2	E, N-m	K
1	0.051875	0.062500	0.83	4744.53	8955.76	400.31	460.01	52.50	6,480,203.20	0.28
2	0.006250	0.062500	0.10	3062.01	8381.99	298.72	460.01	44.72	2,299,252.87	0.13
3	0.069098	0.083250	0.83	4744.53	8955.76	533.22	460.01	69.93	8,631,630.67	0.28
4	0.008250	0.083250	0.10	3062.01	8381.99	397.89	460.01	59.57	3,062,604.82	0.13
5	0.103750	0.125000	0.83	4744.53	8955.76	800.63	460.01	105.00	12,960,406.41	0.28
6	0.012500	0.125000	0.10	3062.01	8382.00	597.44	460.01	89.44	4,598,505.73	0.13
7	0.207500	0.250000	0.83	4744.53	8955.76	1601.26	460.01	209.99	25,920,812.81	0.28
8	0.025000	0.250000	0.10	3061.98	8381.99	1194.87	460.01	178.89	9,196,839.37	0.13
9	0.062500	0.051875	1.20	5173.35	9091.92	353.26	460.01	44.95	6,596,771.95	0.33
10	0.062500	0.006250	10.00	6677.49	10217.65	65.50	460.01	6.60	1,613,534.13	0.43
11	0.083250	0.069098	1.20	5173.35	9091.92	470.54	460.01	59.87	8,786,900.23	0.33
12	0.083250	0.008325	10.00	6750.67	10217.64	87.25	460.01	8.79	2,196,589.33	0.44
13	0.125000	0.103750	1.20	5173.35	9091.92	706.52	460.01	89.90	13,193,543.89	0.33
14	0.125000	0.012500	10.00	6766.89	10217.65	131.00	460.01	13.20	3,314,054.15	0.44
15	0.250000	0.207500	1.20	5173.35	9091.92	1413.03	460.01	179.80	26,387,087.77	0.33
16	0.250000	0.025000	10.00	6428.03	10217.65	262.00	460.01	26.40	5,980,916.13	0.40

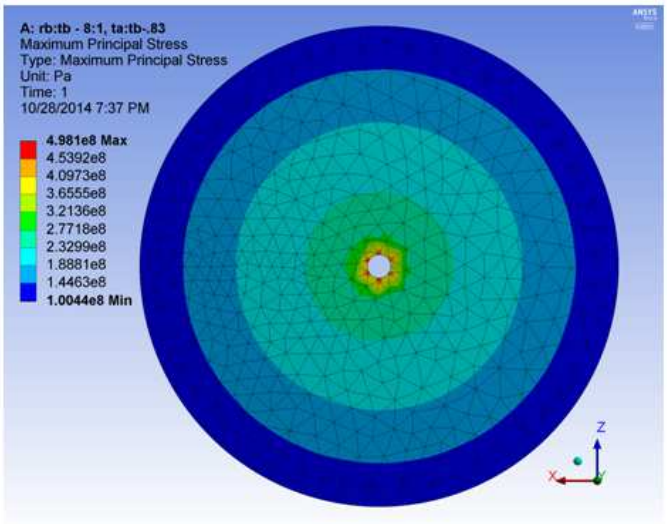

Fig. 4. Case #1-hoop stress

DOI: 10.3844/erjsp.2015.54.63

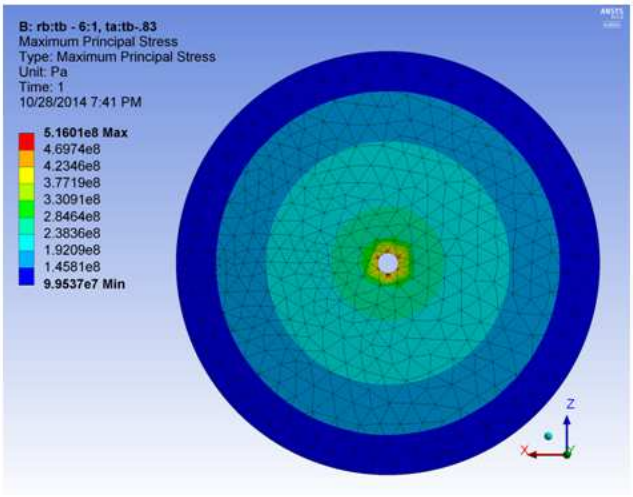

Fig. 5. Case #3-hoop stress

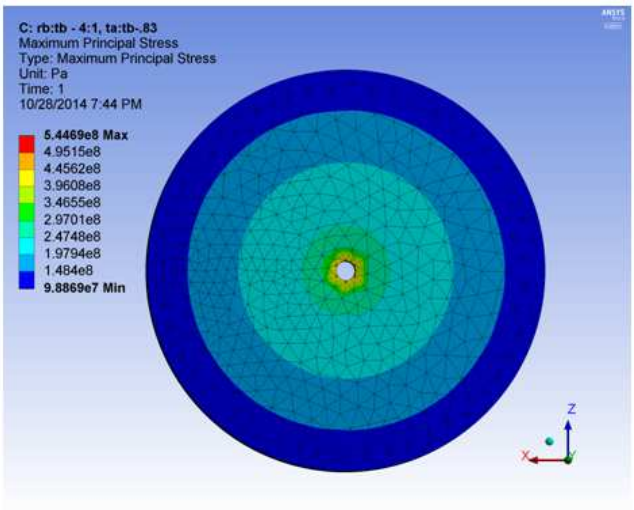

Fig. 6. Case #5-hoop stress

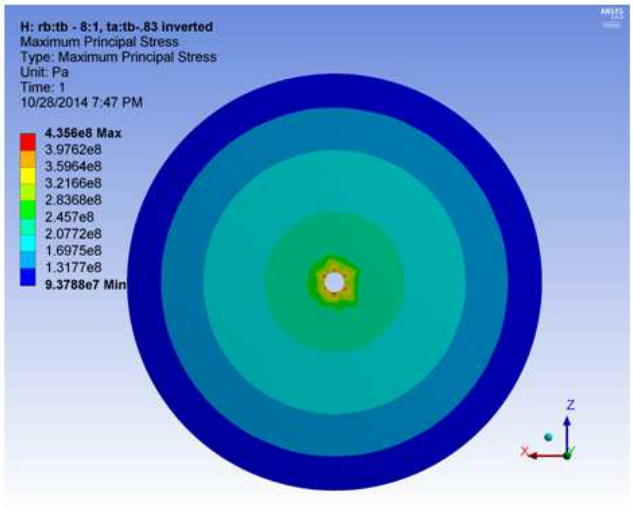

Fig. 7. Case #9 – hoop stress

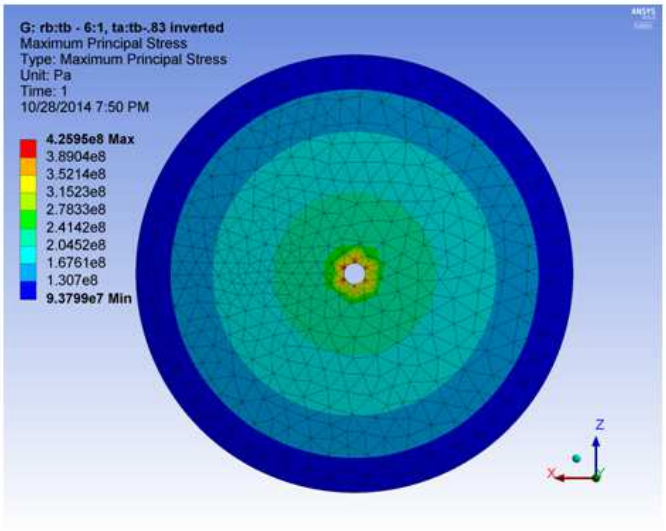

Fig. 8. Case #11-hoop stress

For large thickness ratios, i.e. case #16, ANSYS proved to generate more conservative hoop stress than the analytical Equations (5) and (6). Using ANSYS, in this case, will prevent over valuing of the shape factor and the operating speeds of the flywheel. Based on a table of shape factors given in Kousksou *et al*. (2014), flywheel shapes similar to Profile #2, has a much higher shape factor than the factor presented in Table 5. Profile #2 should have a shape factor closer to 0.70 or higher. If Equations (5) and (6) were used for case #16, it would actually produce a *K* value of 0.74. The constraints used in ANSYS are the likely reason for this discrepancy.

Conclusion

The influence of various geometric configurations of flywheels on energy storage performance was examined. Utilizing both analytical stress equations and finite element analysis via ANSYS, together, in the flywheel profile analysis was useful in that they served as a results "check" to see if one method of analysis is more useful than the other for particular thickness ratios. In particular, for larger thickness ratios ANSYS can be used to prevent overestimating the shape factor and the operating speed of the flywheel, since ANSYS generates more conservative hoop stress than the analytical stress.

Although the resulting shape factors are low for the profiles chosen, the energy storage capabilities of Profile #1 are large enough to be still considered for use in a flywheel storage system.

As a future research topic for flywheels, modal, or frequency analysis of flywheels would provide useful information in the case of more complicated flywheel designs. Also, research into reverse engineering a flywheel, i.e. designing a flywheel for a specific operating speed and energy storage capability, would streamline the design process and produce custom flywheels for any specific application.

Acknowledgment

A special acknowledgement to the late William Kinsel who dedicated his life to teaching engineering.

Author's Contributions

Shenel Bankston: Performed the research and calculations to support the data represented.

Changki Mo: Acted as the academic advisor and checked the content for consistency and accuracy.

Ethics

There are no ethical issues generated from the data or information presented in this study.

References

Arslan, M.A., 2008. Flywheel geometry design for improved energy storage using finite element analysis. Material Design, 29: 514-518. DOI: 10.1016/j.matdes.2007.01.020

Bitterly, J.G., 1998. Flywheel technology: Past, present and 21st century projections. IEEE AES Syst. Magazine, 13: 13-16. DOI: 10.1109/62.707557

Bolund, B., H. Bernhoff and M. Leijon, 2007. Flywheel energy and power storage systems. Renewable Sustainable Energy Rev., 11: 235-258. DOI: 10.1016/j.rser.2005.01.004

Genta, G., 1985. Kinetic Energy Storage: Theory and Practice of Advanced Flywheel Systems. 1st Edn., Butterworths, London, ISBN-10: 0408013966, pp: 362.

Kousksou, T., P. Bruel, A. Jamil, T. El Rhafiki and Y. Zeraouli, 2014. Energy storage: Applications and challenges. Solar Energy Mater. Solar Cells, 120: 59-80. DOI: 10.1016/j.solmat.2013.08.015

Liu, H. and J. Jiang, 2007. Flywheel energy storage-an upswing technology for energy sustainability. Energy Buildings, 39: 599-604. DOI: 10.1016/j.enbuild.2006.10.001

Moore, C.J. and T.G. Kraft, 2012. Metallic Rotor Sizing and Performance Model for Flywheel Systems. 1st Edn., NASA/TM-2012-217808, Glenn Research Center, Cleveland, Ohio.

Pena-Alzola, R., R. Sabastian, J. Quesada and A. Colmenar, 2011. Review of flywheel based energy storage systems. Proceedings of the International Conference on Power Engineering, Energy and Electrical Drives, May 11-13, IEEE Xplore Press, Malaga, pp: 1-6. DOI: 10.1109/PowerEng.2011.6036455

Pochiraju, A., 2012. Design principles of a Flywheel Regenerative Braking System (F-RBS) for formula SAE type racecar and system testing on a virtual test rig modeled on MSC ADAMS. University of Kansas School of Engineering, Lawrence.

Ugural, A.C. and S.K. Fenster, 2011. Advanced Mechanics of Materials and Applied Elasticity. 1st Edn., Prentice Hall, Upper Saddle River, NJ, ISBN-10: 0137079206, pp: 680.

You, L.H., Y.Y. Tang, J.J. Zhang and C.Y. Zheng, 2000. Numerical analysis of elastic-plastic rotating disk with arbitrary variable thickness and density. Int. J. Solids Structures, 37: 7809-7820. DOI: 10.1016/S0020-7683(99)00308-X